AIAA JOURNAL
Vol. 48, No. 1, January 2010

Optimization of Variable-Stiffness Panels for Maximum Buckling Load Using Lamination Parameters

Samuel T. IJsselmuiden,* Mostafa M. Abdalla,† and Zafer Gürdal‡
Delft University of Technology, 2629 HS Delft, The Netherlands

DOI: 10.2514/1.42490

With the large-scale adoption of advanced fiber placement technology in industry, it has become possible to fully exploit the anisotropy of composite materials through the use of fiber steering. By steering the composite fibers in curvilinear paths, spatial variation of stiffness can be induced resulting in beneficial load and stiffness distribution patterns. One especially relevant area in which fiber steering has proved its effectiveness is in improving buckling loads of composite panels. Previous research used predefined forms of fiber angle variations and the coefficients of these analytic expressions were used as design variables. Alternatively, the local ply angles were used as design variables directly. In this paper, a framework is developed to treat the most general approach that considers the largest possible design space. The use of lamination parameters efficiently defines stiffness variation over a structural domain with the minimum number of variables. A conservative reciprocal approximation scheme is introduced. The inverse buckling factor is expanded linearly in terms of the in-plane stiffness and in terms of the inverse bending stiffness. The new approximation scheme is convex in lamination parameter space. Numerical results demonstrate improvements in excess of 100% in buckling loads of variable-stiffness panels compared to the optimum constant stiffness designs. Buckling load improvements are attributed primarily to in-plane load redistribution, which is confirmed both by the prebuckling stress distribution as well as by comparing the performance of designs optimized with variation of both in-plane and bending stiffness to those optimized with only bending stiffness variation. A tradeoff study between in-plane stiffness and buckling performance is also presented and shows the benefits of variable-stiffness design in enlarging the design possibilities of composite panels.

I. Introduction

BUCKLING design of laminated composite plates is well studied in the literature [1–3]. Research has shown that significant structural performance improvements are possible when tailoring the local stiffness properties of composite laminates [4–9].

In the past, several different strategies have been adopted to parametrize and study local stiffness variations in composite structures, one form of which was based on steered fiber paths. Gürdal and Olmedo [5] parametrized fiber paths using linear fiber angle variation. Tatting and Gürdal [6] and Jegley et al. [10] used linear variation fiber path definitions to design, manufacture, and test variable-stiffness panels. Blom et al. [11] used geodesic, constant angle, and constant curvature definitions to prescribe fiber paths over a conical shell. Honda et al. [12] used parabolic fiber paths to study the vibration of composite plates. The advantage of these approaches is that only a few design variables are needed and fiber continuity is guaranteed, at the expense of a limited design space. The design space can be enlarged by expressing fiber paths in terms of Lobatto polynomials, as was done by Alhajahmad et al. [13].

Apart from direct parameterization of fiber angle variation, some investigators used local design variables at the element or node level. Hyer and Lee [4] studied the influence of stiffness tailoring on a panel with a hole by dividing a model into several elements, each having its own discrete fiber orientation. Similarly, Setoodeh et al. [14] used nodal-based fiber angles as design variables. Associating design variables with elements (or nodes) has the advantage of providing the largest possible design space for a given mesh density. The drawback of this approach is that fiber continuity is difficult to impose when fiber angles are used as design variables.

Lamination parameters have been used successfully for variable-stiffness designs in the past. Abdalla et al. [9] and Setoodeh et al. [8] presented design methods based on lamination parameters to optimize fundamental frequency and stiffness of composite plates. Lamination parameters allow the local stiffness properties to be described using a finite set of continuous design variables, without requiring explicit knowledge of the final stacking sequence [15,16]. This reduces the number of required design variables needed to describe any given design without limiting the design space. Since the individual fiber angles do not need to be prescribed the analysis is further simplified as the continuity of ply angles between adjacent elements does not have to be explicitly taken into consideration.

Postprocessing is required to determine the actual fiber angle distribution from a lamination parameter-based solution. Traditionally, the Lipton algorithm [17] was used to determine three ply angles and corresponding thicknesses for constant stiffness laminates. This procedure is, however, not applicable when considering variable-stiffness laminates. Honda and Narita [18] presented a method of defining the local stacking sequences per element to match lamination parameters found after minimizing the out-of-plane deflection of a plate. Setoodeh et al. [19] applied curve-fitting techniques based on Lobatto polynomials and were able to generate continuous fiber paths suitable for manufacturing using fiber placement machines.

In this paper, a conservative approximation scheme [20] is presented for the design of variable-stiffness composite panels for maximum buckling load. The approximation expresses the buckling load as a linear combination of the in-plane and bending stiffness tensors and the corresponding inverses. The present work builds on work presented by Setoodeh et al. [14] where a variable-stiffness panel was designed using fiber angles to improve buckling performance. The approximation scheme is improved to guarantee homogeneity in stiffness space and convexity in lamination parameter space. The developed approximation scheme retains the desirable properties of the earlier version including being separable. The adjoint method is used to compute the sensitivity of all the design variables, requiring only one back substitution using the already factored in-plane stiffness matrix. The dual-formulation method is used in the case that repeated eigenvalues are present.

Presented as Paper 2123 at the 49th AIAA/ASME/ASCE/AHS/ASC Structures, Structural Dynamics, and Materials Conference, Schaumburg, IL, 7–10 April 2008; received 2 December 2008; revision received 17 August 2009; accepted for publication 8 September 2009.

*Ph.D. Student. Member AIAA; s.t.ijsselmuiden@tudelft.nl.
†Assistant Professor. Member AIAA.
‡Professor, Aerospace Structures Chair. Associate Fellow AIAA.

In the next section the finite element formulation used for buckling analysis is presented followed by a short discussion on lamination parameters and their feasible region. In Sec. III the new conservative approximation scheme for buckling is developed. The optimization formulation for buckling load maximization is presented, as well as the formulation to study the tradeoff between stiffness and buckling. Two example problems taken from literature are studied in Sec. IV demonstrating the advantage of variable-stiffness designs as well as confirming load redistribution as the primary mechanism for improved buckling performance.

II. Buckling Analysis

The buckling load is determined using a finite element discretization of the buckling analysis through the following eigenvalue problem:

$$(\mathbf{K}^b - \lambda \mathbf{K}^g) \cdot \mathbf{a} = \mathbf{0} \tag{1}$$

where $\mathbf{K}^b$ is the global bending stiffness matrix, $\mathbf{K}^g$ is the global geometric stiffness matrix, $\mathbf{a}$ is the mode shape comprising deformation degrees of freedom, and λ is the load multiplier (or buckling factor). The mode shapes are normalized such that

$$\mathbf{a}^T \cdot \mathbf{K}^b \cdot \mathbf{a} = 1 \tag{2}$$

The geometric stiffness matrix is constructed through an assembly of element geometric matrices. The stiffness matrix of each element takes the form

$$\mathbf{K}_e^g = -n_x \mathbf{K}^x - n_y \mathbf{K}^y - n_{xy} \mathbf{K}^{xy} \tag{3}$$

where $\mathbf{n}_e = (n_x, \quad n_y, \quad n_{xy})^T$ is the vector of in-plane stress resultants averaged over the element, and $\mathbf{K}^x$, $\mathbf{K}^y$, and $\mathbf{K}^{xy}$ are constant matrices that depend only on element geometry.

The averaged in-plane stress resultants can be expressed as

$$\mathbf{n}_e = \mathbf{A}_e \cdot \mathbf{e}_e \tag{4}$$

where $\mathbf{A}$ is the in-plane stiffness matrix and $\mathbf{e}$ is the average strain vector given by

$$\mathbf{e}_e = \bar{\mathbf{B}}_e \cdot \mathbf{u}_e \tag{5}$$

where $\mathbf{u}$ is the vector of in-plane displacements, $\mathbf{u}_e$ is the vector of the degrees of freedom associated with nodes connected to the eth element, and $\bar{\mathbf{B}}$ is the average element strain displacement matrix (see Appendix B for the definitions). The in-plane displacements can be found from the solution of the in-plane equilibrium equations:

$$\mathbf{K}^m \cdot \mathbf{u} = \mathbf{f} \tag{6}$$

where f is the vector of in-plane loads.

A. Interpolation Scheme

An important aspect of designing variable-stiffness panels is to ensure the continuity of the lamination parameter distribution. Intuitively, design variables are associated directly with the elements when using a finite element approach. However, when independent design variables are assigned per element, there is no guarantee that the lamination parameter distribution is going to be continuous.

To ensure the smoothness of the solution the design variables are associated with the nodes rather than elements. The stiffness properties of the elements are subsequently computed by averaging the value of the nodal compliance values. This approach, first introduced by Abdalla et al. [9], has been effective in producing smooth lamination parameter distributions. The average element compliance is given by

$$\bar{\mathbf{A}}_e^{-1} = \sum_{i \in \mathcal{I}_e} w_{e,i} \mathbf{A}_i^{-1} \tag{7}$$

where i denotes the node numbers and $\mathcal{I}_e$ is the set of nodes connected to element e. The sum is weighed by integration weighing coefficients w_e such that for a smooth function f,

$$\int_{\Omega_e} f \, \mathrm{d}\Omega \approx \int_{\Omega_e} \mathrm{d}\Omega \sum_{i \in \mathcal{I}_e} w_{e,i} f_i \tag{8}$$

Similar expressions are used for interpolating the inverse of the bending stiffness matrix.

B. Lamination Parameters

Stiffness properties of any given laminate can be uniquely defined by a set of 12 continuous parameters known as lamination parameters. For symmetric laminates, eight parameters are sufficient. Imposing an additional balanced condition reduces the number of parameters to four. Initially introduced by Tsai and Pagano [15] and Tsai and Hahn [16], the in-plane and out-of-plane lamination parameters are defined as

$$(V_1, V_2, V_3, V_4) = \int_{-1/2}^{1/2} (\cos 2\theta(\bar{z}), \sin 2\theta(\bar{z}), \cos 4\theta(\bar{z}), \sin 4\theta(\bar{z})) d\bar{z} \tag{9}$$

$$(W_1, W_2, W_3, W_4) = 12 \int_{-1/2}^{1/2} \bar{z}^2 (\cos 2\theta(\bar{z}), \sin 2\theta(\bar{z}), \cos 4\theta(\bar{z}), \sin 4\theta(\bar{z})) d\bar{z} \tag{10}$$

where $\bar{z} = z/h$ is the normalized through-the-thickness coordinate of the layers [21], h is the total thickness of the laminate, and $\theta(\bar{z})$ is the fiber angle at $\bar{z}$. The in-plane laminate stiffness matrix $\mathbf{A}$ and the bending stiffness matrix $\mathbf{D}$ can subsequently be defined as a linear function of the lamination parameters:

$$\mathbf{A} = h(\boldsymbol{\Gamma}_\mathbf{0} + V_1 \boldsymbol{\Gamma}_\mathbf{1} + V_2 \boldsymbol{\Gamma}_\mathbf{2} + V_3 \boldsymbol{\Gamma}_\mathbf{3} + V_4 \boldsymbol{\Gamma}_\mathbf{4}) \tag{11}$$

$$\mathbf{D} = \frac{h^3}{12} (\boldsymbol{\Gamma}_\mathbf{0} + W_1 \boldsymbol{\Gamma}_\mathbf{1} + W_2 \boldsymbol{\Gamma}_\mathbf{2} + W_3 \boldsymbol{\Gamma}_\mathbf{3} + W_4 \boldsymbol{\Gamma}_\mathbf{4}) \tag{12}$$

where Γ_i $(i = 1, \ldots, 4)$ are matrices in terms of laminate invariants, defined in Appendix A.

The feasible region for lamination parameters is well defined [22] when solving design problems that are dependent only on in-plane or out-of-plane lamination parameters. However, if stiffness is allowed to vary over the domain, the buckling load is not only a function of the bending stiffness $\mathbf{D}$ but also of the in-plane stiffness $\mathbf{A}$ [23]. Thus, a feasible region of the combined in-plane and out-of-plane lamination parameters is required. Currently, no analytical expression for the combined feasible domain is known; therefore, it is approximated using a set of linear constraints obtained from successive convex hull approximations of the design space as described by Setoodeh et al. [24].

III. Conservative Approximation Formulation

Successive approximation techniques are popular in structural optimization as they increase computational efficiency by reducing the number of structural analyses required to find an optimum. The idea is to create a separable approximation of the objective function and constraints where each term in the approximation depends on the design variables associated with one node (or element). The optimization is carried out on the approximation after which the design is updated and the procedure is repeated until a converged solution is found. The approximate subproblem is usually solved using a dual approach [20,25].

The buckling load factor is a function of both the in-plane stiffness and the bending stiffness, i.e. $\lambda(\mathbf{A}, \mathbf{D})$. In past research the generalized reciprocal approximation, in which the response is approximated based on the inverse of the stiffness tensors, has been successful for variable-stiffness design [9,26]. Applying the same approach for buckling design has been difficult, since the approximation is found to be nonhomogeneous and nonconvex [14]. The approximation was treated in [14] in the context of buckling load

minimization using fiber angles as design variables. Convexity in lamination parameter space is much easier to reinforce [9,26,27]. In this section, we develop a convex approximation for buckling load factors that derives insight from the homogeneity properties of the buckling factors as functions of the in-plane and bending stiffness tensors.

The effect of the in-plane and out-of-plane stiffness on the buckling load can be treated as two individual parts. This is best clarified by inspecting the sensitivity of the critical eigenvalue with respect to an arbitrary design variable. The variable b is assumed to affect only the local stiffness properties of a single element, i. The expression of the sensitivity is obtained by differentiating Eq. (1) and can be written as [20]

$$\frac{d\lambda}{db} = \lambda \mathbf{a}^T \cdot \left(\frac{d\mathbf{K}^b}{db} - \lambda \frac{d\mathbf{K}^g}{db} \right) \cdot \mathbf{a} \tag{13}$$

and is composed of two terms. The first term is dependent on the derivative of the bending stiffness and is local, which implies information from a single element is sufficient to evaluate its influence on the critical buckling factor. The second term, which is the derivative of the geometric stiffness, is not local. The in-plane loads of all elements are influenced by changing the stiffness of a single element and therefore the geometric stiffness matrices of all elements would change. The second term essentially represents the effect of load redistribution within the plate.

Further insight into the dependency of the buckling factor on in-plane and bending stiffness can be gained by inspecting Eqs. (1–6). The buckling factor is a homogeneous function of order zero with respect to the in-plane stiffness as can be verified by noting the effect of scaling the stiffness terms in Eq. (6) by a constant factor. The resulting displacements (and strains) would be multiplied by the inverse of that factor and hence the in-plane stresses [Eq. (4)] would remain unchanged. The physical meaning is that buckling load factor depends on load redistribution, which occurs due to a relative change in the in-plane stiffnesses over the domain. On the other hand, the buckling load factor is homogeneous of order one with respect to the bending stiffness. These homogeneity properties can be also expressed in terms of the inverse buckling factor $r = 1/\lambda$, a measure of structural compliance, which is homogeneous of order zero with respect to the in-plane stiffness and of order one with respect to *inverse* bending stiffness.

A homogenous approximation is obtained by expanding the inverse buckling factor. The inverse buckling factor is expanded linearly in terms of in-plane stiffnesses and the inverse bending stiffnesses, resulting in the following expression:

$$r \approx \hat{r} + \sum_{i=1}^{N} \left[\frac{\widehat{\partial r}}{\partial \mathbf{A}_i} : (\mathbf{A}_i(\mathbf{V}) - \hat{\mathbf{A}}_i) + \frac{\widehat{\partial r}}{\partial \mathbf{D}_i^{-1}} : (\mathbf{D}_i^{-1}(\mathbf{W}) - \hat{\mathbf{D}}_i^{-1}) \right] \tag{14}$$

where the $\hat{}$ represents the design point about which the inverse buckling factor is expanded and $i = 1 \ldots N$ are the nodes or elements for which the design variables are defined. The : operator represents matrix inner product.

Euler's theorem for homogeneous functions implies that, at any approximation point, the sum over all nodes for the in-plane stiffness contributions is always zero; that is,

$$\sum_{i=1}^{N} \left(\frac{\partial r}{\partial \mathbf{A}_i} : \mathbf{A}_i \right) = 0 \tag{15}$$

while the corresponding sum of bending terms gives the inverse buckling factor:

$$\sum_{i=1}^{N} \left(\frac{\partial r}{\partial \mathbf{D}_i^{-1}} : \mathbf{D}_i^{-1} \right) = r \tag{16}$$

The final form of the approximation reduces to

$$\frac{1}{\lambda} \approx \sum_{i=1}^{N} [\boldsymbol{\Psi}_i^m : \mathbf{A}_i + \boldsymbol{\Phi}_i^b : \mathbf{S}_i] \tag{17}$$

where $\boldsymbol{\Psi}^m$ and $\boldsymbol{\Phi}^b$ are the sensitivity tensors with respect to in-plane stiffness and the inverse bending stiffness, respectively, as defined in Appendix C. The sensitivity tensors $\boldsymbol{\Psi}^m$ satisfy [cf. Equation (15)]

$$\sum_{i=1}^{N} \boldsymbol{\Psi}_i^m : \mathbf{A}_i = 0 \tag{18}$$

Since the in-plane stiffness tensor is always positive definite, Eq. (18) implies that the sensitivity tensors $\boldsymbol{\Psi}^m$ are not necessarily definite. This lack of definiteness is not problematic since the $\boldsymbol{\Psi}^m$ appear only in linear terms. On the other hand, as shown in Appendix C, the sensitivity tensors $\boldsymbol{\Phi}^b$ are always positive definite, and therefore the approximation as a whole is guaranteed to be convex [24]. The proposed approximation is a generalization of the conservative approximation [20] where a hybrid formulation of the linear and the reciprocal approximation techniques is used. The detailed derivation of the sensitivity matrices is shown in Appendix C.

In work previously published by the authors [14] the variable-stiffness buckling optimization problem was parametrized in terms of fiber angles, resulting in a nonconvex design problem. As was suggested earlier, introducing lamination parameters as design variables results in a convex design space. However two important observations have been made with respect to formulating an approximation scheme. In the aforementioned work the buckling factor was approximated directly using a reciprocal approximation. First, this resulting approximation is nonhomogenous. Second, the convexity of the terms dependent on in-plane stiffness cannot be guaranteed if the reciprocal is used as the sensitivities will not necessarily be positive definite. The approximation scheme [Eq. (25)] presented in this paper reproduces the homogeneity properties of the buckling factor and is convex. Thus, the proposed approximation is a suitable starting point for a successive approximation optimization methodology.

A. Optimization Formulation

When considering straight fiber composite designs an improvement in buckling performance can result in a deterioration of the overall in-plane stiffness performance [23]. It is therefore interesting to study the tradeoff between in-plane stiffness design optimization and buckling performance optimization of variable-stiffness laminates. The structural stiffness can be maximized by minimizing the compliance [22,24]. Using a similar approximation approach as for buckling, the compliance can be formulated as

$$C \approx \sum_{i=1}^{N} \boldsymbol{\Phi}_i^m : \mathbf{A}_i^{-1} \tag{19}$$

where in this case $\boldsymbol{\Phi}^m$ is the sensitivity of the in-plane stiffness with respect to the change in compliance of the considered node. The derivation of the sensitivity matrix is available at the end of Appendix C.

The combined buckling-stiffness optimization problem can hence be formulated as

$$\min_{\mathbf{v},\mathbf{w}} \left(\alpha \cdot \frac{\lambda_{\text{cr}}^*}{\lambda_{\text{cr}}} + (1 - \alpha) \cdot \frac{C}{C^*} \right) \tag{20}$$

where λ_{cr}^* and C^* are arbitrary reference values used to normalize the critical buckling load, λ_{cr}, and the stiffness, C. The relative importance of either the buckling load or stiffness is controlled via a predefined coefficient α having a value between ϵ and $1 - \epsilon$, where ϵ is a small parameter, allowing us to study the tradeoff between stiffness and buckling performance.

The approximations in Eqs. (17) and (19) are separable and thus can be solved locally at each node. The local optimization problem can therefore be formulated as

$$\min_{\mathbf{v}_i,\mathbf{w}_i}\left[\alpha\lambda^*_{\mathrm{cr}}\cdot(\boldsymbol{\Psi}^m_i{:}\mathbf{A}_i+\boldsymbol{\Phi}^b_i{:}\mathbf{S}_i)+\frac{(1-\alpha)}{C^*}\cdot\boldsymbol{\Phi}^m_i{:}\mathbf{R}_i\right] \tag{21}$$

subject to the constraints imposed by the feasible region of the lamination parameters.

Several issues are worth mentioning at this point. First, it is worth noting that the Pareto front representing the tradeoff between buckling and stiffness is not necessarily convex. Thus, in practice, points on the Pareto front are obtained by iteratively updating the design according to Eq. (21). While the iteration converges to a local minimum of the approximation, it is guaranteed only to be a stationary point of the objective function (20). This means that the iteration scheme can converge even for the nonconvex portions of the Pareto front.

The second issue is that for α approaching unity, the buckling approximation (17) is not strictly convex, which leads to convergence problems. The third issue is that buckling mode interaction can cause convergence problems if only a single buckling mode is taken into account during the optimization. These last two issues are discussed in the following subsections.

B. Multimodal Design

The formulation presented thus far assumes that only one eigenvalue is present during optimization; however for multimodal problems all critical buckling modes must be incorporated in the design. Multimodal optimization can be achieved using a method similar to the bound formulation proposed by Olhoff [28] by introducing an independent parameter, β, such that the optimization becomes

$$\min\beta \quad \text{s.t.} \quad \beta\geq\frac{1}{\tilde{\lambda}_n} \tag{22}$$

where $\tilde{\lambda}_n$ (for $n=1,2,\ldots N$) are the buckling factors corresponding to the N critical buckling modes. The problem can subsequently be solved using the dual-method [25,29], which leads to the following two conditions:

$$\mathcal{L}_C=\min\sum\frac{\mu_n}{\tilde{\lambda}_n} \quad \text{and} \quad \sum\mu_n=1 \tag{23}$$

where μ_n are the Lagrange multipliers and are determined by maximizing the complimentary Lagrangian subject to nonnegativity of the Lagrange multipliers, $\mu_n\geq 0$, as well as their sum being unity. When multiple buckling modes are present, the approximation of the buckling factor (17) includes the sum of the sensitivities of the active buckling modes:

$$\hat{\boldsymbol{\Phi}}^b_i=\sum_{n=1}^{N}\mu_n\boldsymbol{\Phi}^b_i \quad \text{and} \quad \hat{\boldsymbol{\Psi}}^m_i=\sum_{n=1}^{N}\mu_n\boldsymbol{\Psi}^m_{i,n} \tag{24}$$

C. Proximal Point Algorithm

Even though the proposed approximations are convex, the buckling approximation is not strictly convex. Because of this lack of strict convexity, convergence problems are encountered when maximizing the buckling load factor. The presence of multimodal designs also further compounds the convergence difficulties. The situation can be remedied by regularizing the expression by introducing an additional term that is strictly convex with respect to the in-plane design variables. The proximal point algorithm, following Rockafellar [30], is an effective method of ensuring convergence while retaining a separable approximation. The local optimization problem is therefore expressed as

$$\min_{\mathbf{v}_i,\mathbf{w}_i}\left(\boldsymbol{\Psi}^m_i{:}\mathbf{A}_i+\boldsymbol{\Phi}^b_i{:}\mathbf{S}_i+\frac{\eta}{2}\cdot\mathcal{C}_i\right) \tag{25}$$

where η is a scaling factor, which is free to be defined. The convex term $\mathcal{C}$ is defined as

$$\mathcal{C}_i=\sum_{j=1}^{4}[\|V_{ij}-\tilde{V}_{ij}\|^2+\|W_{ij}-\tilde{W}_{ij}\|^2] \tag{26}$$

Note that the contribution of this term tends to zero as the solution converges. The value chosen for η is constant and in essence represents a move limit for the design variables, hence influencing the speed of convergence. Smaller values of η result in quicker convergence; however as η tends to zero the local approximation may no longer be strictly convex. The choice of η can be made somewhat less arbitrary by considering the approximate gradient of a function $f(\mathbf{x})$ that is being optimized:

$$\nabla f=\nabla\tilde{f}+\eta\cdot\|x_j-\tilde{x}_j\|+(\mathbf{H}+\eta\mathbf{I})\Delta\mathbf{x}=0 \tag{27}$$

where x_i represents the design variables, $\mathbf{H}$ is the Hessian matrix, and $\mathbf{I}$ is the identity matrix. For large values of η, the Hessian matrix becomes negligible. The gradient at the initial point (i.e at $x=\tilde{x}$) is therefore found to be

$$\nabla f=\nabla\tilde{f}+\eta\cdot\mathbf{I}\Delta\mathbf{x} \tag{28}$$

Therefore, if the change in design variables is to be limited to a maximum predefined value, η can be expressed as the maximum gradient over all elements at the initial point divided by the chosen move limit $\|\Delta\mathbf{x}\|$:

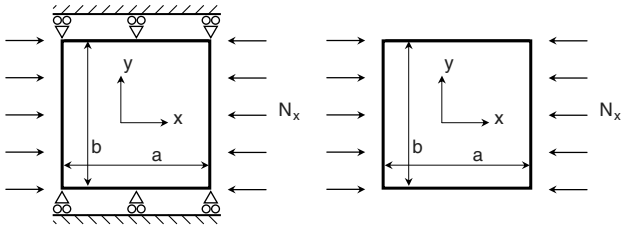

a) Case 1: Simply supported, enforced straight edges, no lateral expansion

b) Case 2: Simply supported, enforced straight edges

Fig. 1 Geometry, loading, and boundary conditions for the considered rectangular plates.

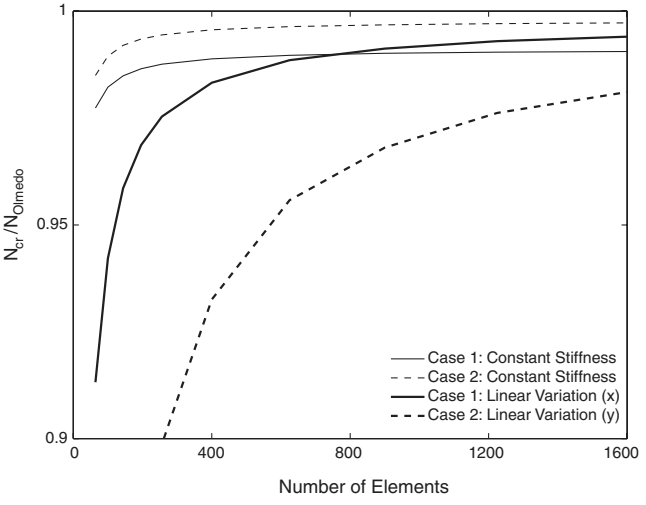

Fig. 2 Mesh convergence of the critical buckling load, normalized with respect to the results presented by Olmedo and Gürdal [23].

Table 1 Optimal dimensionless buckling modes for several laminate configurations for case 1.[a]

	$\tilde{N}_{cr}$ 100 elements				$\tilde{N}_{cr}$ 400 elements			
	Mode 1	Mode 2	Mode 3	%	Mode 1	Mode 2	Mode 3	%
QI, $[\pm 45, 0, 90]_s$	1.0597	1.9865	3.6694	——	1.0681	2.0106	3.7151	—
CS, $[\pm 32]_s$	1.1885	2.6374	2.7023	12	1.1965	2.6669	2.7362	12
LV(x), $\langle 0, 50 \rangle_s$	1.3568	2.4831	3.2501	28	1.4159	2.6835	3.3966	33
VS(x)	1.4890	2.1815	3.9966	41	1.5218	2.2016	4.0966	42
VS(y)	2.3802	2.3803	3.2894	125	2.5634	2.5642	3.4575	140
VS(x, y)	2.4692	2.4705	3.8688	133	2.6492	2.6493	4.0831	148

[a]Improvement percentages are taken with respect to the equivalent quasi-isotropic design ($\tilde{N}_{cr} = N_{cr}a^2/E_1h^3$, QI: quasi-isotropic, CS: constant stiffness, LV: linear variation, VS: variable stiffness)

$$\eta \cdot \|\Delta \mathbf{x}\| = \min_i \nabla f_i(\mathbf{x}^0) \tag{29}$$

The design variables for Eq. (25) are lamination parameters, i.e. $\mathbf{x} \in [-1, 1]$, and hence a reasonable value for the move limit, $\|\Delta \mathbf{x}\|$, of 0.2 to 0.4 can be assumed.

IV. Results

The purpose of this section is to illustrate the benefit of using variable-stiffness design with lamination parameters, as well as to study the mechanisms resulting in improved buckling loads. Two example problems, previously studied by Olmedo and Gürdal [23], are investigated and are outlined in Fig. 1. Both problems consist of a simply supported rectangular plate subject to axial compression introduced via uniform edge displacement. For case 1 (Fig. 1a) the edges remain straight and the panel is prevented from expanding in the lateral direction. The constraint on lateral expansion is removed for the second case (Fig. 1b). A square configuration ($a/b = 1$) is investigated with a 0.06 in.-thick (1.524 mm-thick) laminate based on the following orthotropic material properties:

$$E_{11} = 26.25 \text{ Msi (181 GPa)}, \qquad E_{22} = 1.49 \text{ Msi (10.3 GPa)}$$
$$G_{12} = 1.04 \text{ Msi (7.17 GPa)}, \qquad \nu_{12} = 0.28$$

The plate is discretized into a selected number of equally sized elements and analyzed using a finite element routine programmed in MATLAB. To select the mesh density as well as verify the finite element routine, a mesh convergence study is conducted. In Fig. 2 the number of elements versus the buckling load for the constant stiffness and variable-stiffness designs is plotted for both problem cases. The buckling load is normalized with respect to the results found by Olmedo and Gürdal [23]. Two clear observations can be made; first, variable-stiffness designs require a significantly larger number of elements to converge. This is attributed to the fact that more elements are required to accurately describe the stiffness distribution over the panel. Second, in all cases the buckling load converges to a smaller value than that found by the aforementioned authors. Olmedo and Gürdal applied the Ritz method to solve the buckling problem, which, for a finite set of coefficients, results in a slight overestimate of the actual buckling load.

Design variables are defined at the nodes; therefore the mesh density influences the resolution of the found solution. For this reason the example problems are solved with two different mesh densities, 100 and 400 elements, respectively, to assess the influence of the increased number of elements on the represented optimal solution. Because of the relatively high computational expense, higher mesh densities are currently not considered.

Buckling results are benchmarked against a quasi-isotropic plate, the optimum $[\pm\theta]_s$ design and the optimum linear variation results found by Olmedo and Gürdal [23]. Two different levels of stiffness variation are implemented to evaluate the influence of variable-stiffness design on the buckling performance of a plate. The first level only allows the stiffness to vary along one axis of the plate; in other words the stiffness along the x-axis (loading direction) will remain constant while it varies along the y-axis or vice versa. The optimization is carried out using the formulation developed in Sec. III. The only modification is that the sensitivities along the constant stiffness axis must be summed. The second level allows the stiffness to vary freely over the entire domain, and hence represents the "absolute" variable-stiffness optimum. In all cases the laminates are considered to be locally balanced and symmetric.

Normalized buckling loads and improvement with respect to the quasi-isotropic design for the first and second cases are presented in Tables 1 and 2 respectively. Two general trends are clearly notice-

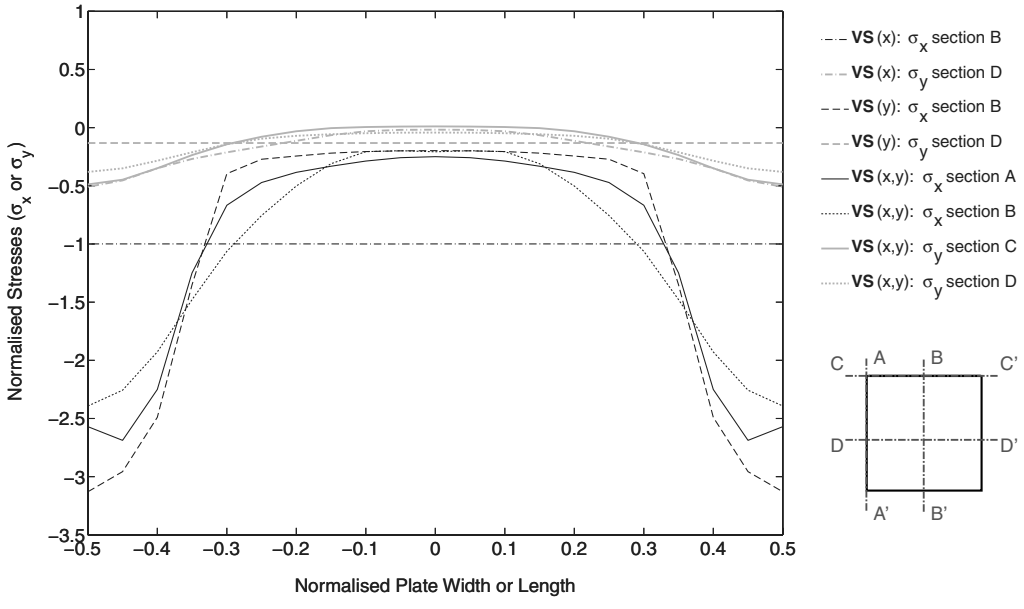

Fig. 3 Normalized stress distribution along several sections for case one.

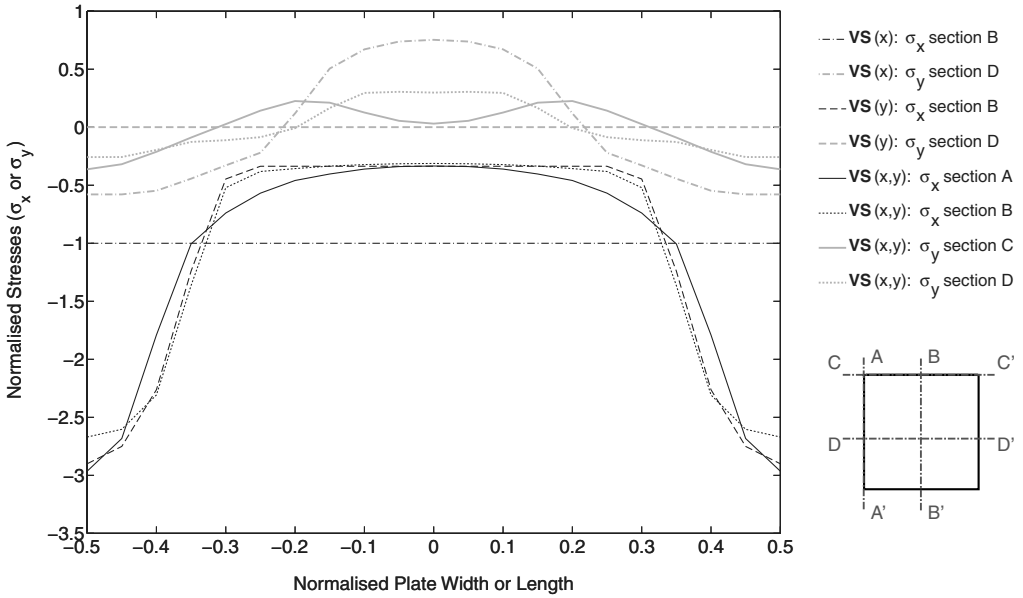

Fig. 4 Normalized stress distribution along several sections for case 2.

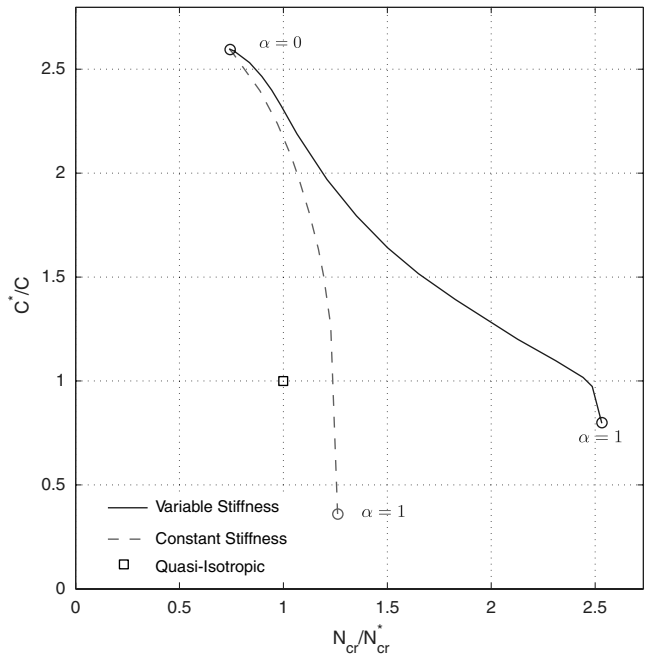

Fig. 5 Pareto front for stiffness ($\alpha = 0$) versus buckling ($\alpha = 1$) optimal designs for both variable and constant stiffness laminates. Values are generated using a 100-element finite element model, and are normalized with respect to a quasi-isotropic laminate.

able; first, when the stiffness is allowed to vary normal to the applied load, i.e. VS(y) and VS(x, y), the largest design improvements are achieved. This indicates that in-plane load redistribution has an important contribution to the improved buckling load, thus affirming the discussion in Olmedo and Gürdal [23]. Second, case 2 is more sensitive to mesh refinement, as the difference between the course and fine mesh are larger than for case one. Figure 2 also indicates that a finer mesh of more than 1600 elements is necessary to capture all the details for case 2.

For case one, Table 1, performance improvements of up to 148% with respect to the quasi-isotropic panel and over 100% with respect to the optimum constant stiffness design are obtained. Increasing the number of elements yields improved results due to the increased number of design variables and improved representation of the stiffness variations. Varying stiffness only along the y-axis yields results within a few percent of full variable-stiffness designs.

Results for case 2, presented in Table 2, show that improvements of nearly 190% are possible. The difference between VS(y) and VS(x, y) are more pronounced for case 2 as lateral load redistribution plays a more important role, as will be seen later. It is also interesting to note that for most of the variable-stiffness designs the first and second buckling modes coincide, reinforcing the necessity of including multiple modes in the design routine.

To gain more insight into the effects of stiffness variation on in-plane load redistribution, the prebuckling stresses along several panel cross sections are plotted in Figs. 3 and 4 for case one and two, respectively. The stresses are normalized by dividing by the magnitude of the prebuckling stress value for a constant stiffness plate. Several different sections along the plate are considered; A − A′ and B − B′ are vertical sections (normal to the loading direction) along the edge and center of the plate, whereas C − C′ and D − D′ are

Table 2 Optimal dimensionless buckling modes for several laminate configurations for case 2.[a]

	$\tilde{N}_{cr}$-100 Elements				$\tilde{N}_{cr}$-400 Elements			
	Mode 1	Mode 2	Mode 3	%	Mode 1	Mode 2	Mode 3	%
QI, $[\pm 45, 0, 90]_s$	1.3734	2.1334	3.7899	—	1.3842	2.1594	3.8373	—
CS, $[\pm 45]_s$	1.7316	2.2900	3.5099	26	1.7424	2.3161	3.5586	26
LV(y), $\langle 90, 15 \rangle_s$	2.4250	2.4639	3.3500	77	2.9282	2.9499	4.0092	112
VS(x)	2.4278	2.4284	4.1722	77	2.5271	2.5271	4.2514	83
VS(y)	3.3121	3.6135	5.0002	141	3.5355	3.8054	5.1586	155
VS(x, y)	3.4773	3.4775	4.7799	153	3.9989	4.0473	5.2261	189

[a]Improvement percentages are taken with respect to the equivalent quasi-isotropic design ($\tilde{N}_{cr} = N_{cr}a^2/E_1h^3$, QI: quasi-isotropic, CS: constant stiffness, LV: linear variation, VS: variable stiffness).

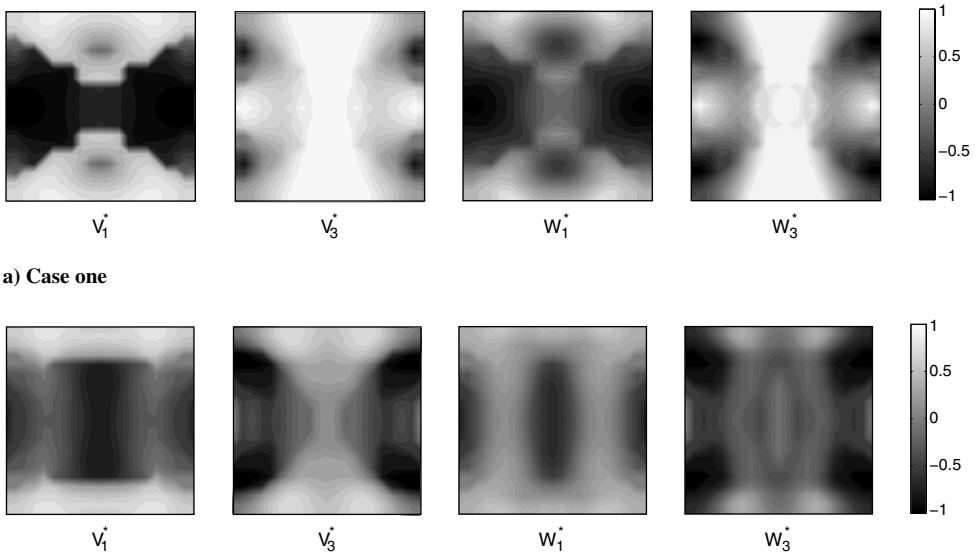

Fig. 6 Optimal lamination parameter distribution for both load cases (for 400 elements).

horizontal sections along the top and center of the plate. The stress distribution along the x-axis, σ_x, is plotted for the vertical sections and the stress distribution along the y-axis, σ_y, is plotted for the horizontal sections.

Similar trends for σ_x are visible for both cases along the vertical sections. Stiffness variation along the x-axis, VS(x), results in constant stress along the plate's width as the stiffness is uniform. For both the case of variable stiffness along the y-axis, VS(y), and full variable stiffness, VS(x, y), for which highest gains in the buckling loads were achieved, the stress distributions are similar. The majority of the compressive stress is concentrated at the edge of the plate, whereas the center of the plate is barely loaded. This clearly demonstrates that the mechanism of load redistribution is primarily responsible for improved buckling load.

The distribution of σ_y along the horizontal sections differs slightly between the two cases. The stress distribution for VS(y) is constant and has a small negative value for case one due to restricted expansion. When stiffness is allowed to vary along the x-axis, VS(x), a similar trend is visible for both cases; the center of the plate is subject to tensile stresses whereas the edges of the plate are compressed. The effect is more pronounced in case 2 as a straight edge condition is enforced while allowing lateral expansion. Even though lateral load redistribution is a secondary effect, it still has a large influence on the buckling load.

To reinforce the argument that buckling load improvements are primarily due to load redistribution the developed optimization routine can be run such that only out-of-plane lamination parameters are considered as design variables. The in-plane lamination parameters are fixed to zero, representing quasi-isotropic in-plane stiffness. For case 2 the optimum normalized buckling load is found to be only 20% higher than that of a quasi-isotropic laminate, which is equivalent to the buckling performance of the equivalent optimal constant stiffness design. However, the full variable-stiffness optimum shows an improvement of almost 190%; thus the largest contribution is deemed to be associated with in-plane stiffness tailoring.

In Sec. III.A, an equation to study the tradeoff between stiffness and buckling was presented, allowing the Pareto front to be computed by varying α over (0, 1). In Fig. 5, the Pareto front for both constant stiffness and variable-stiffness laminates are plotted. The first interesting point to note is that the Pareto front for variables stiffness laminates is not convex; hence uniqueness of the optimal solution is not guaranteed.

When considering designs with high axial stiffness, $\alpha \in (0, 0.3)$, the performance difference between variable and constant stiffness laminates is not large. These designs are dominated by fibers placed parallel to the applied load, leaving little room for stiffness tailoring. As was found in Table 2, the optimum buckling load ($\alpha = 1$) of a variable-stiffness panel is twice that of the constant stiffness design and in excess of 2.5 times that of a quasi-isotropic laminate. Additionally, a variable-stiffness panel with the same in-plane stiffness as a quasi-isotropic plate (i.e., $C^*/C = 1$) can have a buckling load that is almost 150% higher, whereas for a constant stiffness panel the improvement is only around 22%.

It is also interesting to discuss the lamination parameter distribution found for the maximum buckling load, as is shown in Fig. 6. The Miki diagram [31] (Fig. 7) should be kept in mind to interpret the results in Fig. 6. The in-plane stiffness contours, E_x, have been included in the Miki diagram for convenience. For both cases 1 and 2, the regions at the top and bottom edges of the plate for V_1 and $V_3 \approx 1$ refer to values found in the upper-right corner of the Miki diagram, indicating that the plate is axially stiff in these regions. For case one, the center of the plate corresponds to values in the upper-left corner of the Miki diagram, which are axially compliant but stiff in the transverse direction, leading to the slight transverse tensile stresses at the center of the panel as seen in Fig. 3. For case 2, the regions at the center of the plate are values found towards the left boundary of the Miki diagram referring to regions with lower axial stiffness. The values for the out-of-plane lamination parameters are more difficult

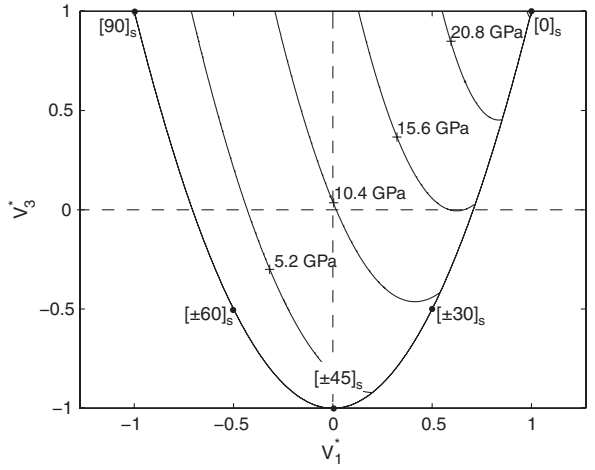

Fig. 7 Miki diagram for the in-plane lamination parameters with contours representing axial stiffness, E_x.

to associate with physical laminate properties, but are included for completeness.

As was mentioned previously, postprocessing is required in order to construct fiber paths from the presented lamination parameter distribution. Van Campen and Gürdal [32] developed a procedure for which they presented the fiber angle distribution for an 8-ply balanced, symmetric laminate corresponding with case 2. Using only two design layers, the authors were able to construct a laminate with comparable performance to the solution presented here.

V. Conclusions

An efficient design approach for variable-stiffness laminates under compressive loads was presented. The design problem was expressed using a separable conservative approximation scheme and the proximal point algorithm was used to ensure convergence of the in-plane parameters. Lamination parameters were used as design variables allowing stiffness and stress distributions to be determined without a priori knowledge of the laminate stacking sequence. Two example problems were studied, yielding buckling load improvements of up to 189% with respect to quasi-isotropic laminates. The stress distribution along several plate sections were presented, confirming that load redistribution is the primary mechanism responsible for improved buckling performance. A tradeoff between axial stiffness and buckling load was also presented. It was shown that a variable-stiffness laminate with in-plane stiffness properties equivalent to a quasi-isotropic plate can be designed to withstand more than twice the compressive load before buckling.

Appendix A: Material Invariants

Lamination parameters allow laminate stiffness properties to be defined as a linear combination of laminate invariant matrices [see Eqs. (11) and (12)]:

$$\Gamma_0 = \begin{bmatrix} U_1 & U_4 & 0 \\ U_4 & U_1 & 0 \\ 0 & 0 & U_5 \end{bmatrix}, \qquad \Gamma_1 = \begin{bmatrix} U_2 & 0 & 0 \\ 0 & -U_2 & 0 \\ 0 & 0 & 0 \end{bmatrix}$$

$$\Gamma_2 = \begin{bmatrix} 0 & 0 & U_2/2 \\ 0 & 0 & U_2/2 \\ U_2/2 & U_2/2 & 0 \end{bmatrix}, \qquad \Gamma_3 = \begin{bmatrix} U_3 & -U_3 & 0 \\ -U_3 & U_3 & 0 \\ 0 & 0 & -U_3 \end{bmatrix}$$

$$\Gamma_4 = \begin{bmatrix} 0 & 0 & U_3 \\ 0 & 0 & -U_3 \\ U_3 & -U_3 & 0 \end{bmatrix}$$

where the laminate invariants, U_i for $i = 1 \ldots 5$, are defined in terms of lamina-reduced stiffnesses by [21]

$$\begin{aligned} U_1 &= (3Q_{11} + 3Q_{22} + 2Q_{12} + 4Q_{66})/8 \\ U_2 &= (Q_{11} - Q_{22})/2 \\ U_3 &= (Q_{11} + Q_{22} - 2Q_{12} - 4Q_{66})/8 \\ U_4 &= (Q_{11} + Q_{22} + 6Q_{12} - 4Q_{66})/8 \\ U_5 &= (Q_{11} + Q_{22} - 2Q_{12} + 4Q_{66})/8 \end{aligned}$$

Appendix B: Definitions for Buckling Analysis

The bending stiffness matrix according to the classical laminate theory is computed as follows [33]:

$$\begin{aligned} \mathbf{K}_e^b = {} & D_{11}\mathbf{T}^{xxxx} + D_{12}(\mathbf{T}^{xxyy} + \mathbf{T}^{yyxx}) + 2D_{16}(\mathbf{T}^{xxxy} + \mathbf{T}^{xyxx}) \\ & + 2D_{26}(\mathbf{T}^{xyyy} + \mathbf{T}^{yyxy}) + 4D_{66}\mathbf{T}^{xyxy} + D_{22}\mathbf{T}^{yyyy} \end{aligned} \tag{B1}$$

where the elements of $\mathbf{T}^{xxxx}$, $\mathbf{T}^{xxyy}$, etc., depend on the element geometry and bending shape functions φ_i:

$$T_{ij}^{\xi\eta\zeta\mu} = \int_{\Omega_e} \frac{\partial^2\varphi_i}{\partial\xi\partial\eta} \frac{\partial^2\varphi_j}{\partial\zeta\partial\mu} dxdy \qquad (i, j = 1, 2, \ldots, 16) \tag{B2}$$

Notice that $d\mathbf{K}_e^b/dD_{\rho\sigma}$ terms as appear in Eq. (C14) can now be easily obtained, for example,

$$\frac{d\mathbf{K}_e^b}{dD_{11}} = \mathbf{T}^{xxxx}, \qquad \frac{d\mathbf{K}_e^b}{dD_{12}} = \frac{\mathbf{T}^{xxyy} + \mathbf{T}^{yyxx}}{2}$$

The in-plane stiffness matrix on the other hand, can be written in the following form:

$$\mathbf{K}_e^m = \begin{bmatrix} \mathbf{k}^{11} & \mathbf{k}^{12} \\ \text{sym.} & \mathbf{k}^{22} \end{bmatrix}$$

The above 4×4 submatrices are given in terms of the laminate extensional stiffness $\mathbf{A}$ as follows [33]:

$$\begin{aligned} \mathbf{k}^{11} &= A_{11}\mathbf{S}^{xx} + A_{16}(\mathbf{S}^{xy} + \mathbf{S}^{yx}) + A_{66}\mathbf{S}^{yy} \\ \mathbf{k}^{12} &= A_{12}\mathbf{S}^{xy} + A_{16}\mathbf{S}^{xx} + A_{26}\mathbf{S}^{yy} + A_{66}\mathbf{S}^{yx} \\ \mathbf{k}^{22} &= A_{66}\mathbf{S}^{xx} + A_{26}(\mathbf{S}^{xy} + \mathbf{S}^{yx}) + A_{22}\mathbf{S}^{yy} \end{aligned} \tag{B3}$$

where the elements of the $\mathbf{S}^{xx}$, $\mathbf{S}^{xy}$, and $\mathbf{S}^{yy}$ matrices depend on the in-plane shape functions ψ_i and are defined as

$$S_{ij}^{\xi\eta} = \int_{\Omega_e} \frac{\partial\psi_i}{\partial\xi} \frac{\partial\psi_j}{\partial\eta} dxdy \qquad (i, j = 1, \ldots, 4)$$

In this paper, only square bilinear elements are used with fixed side length s. Therefore, matrices $\mathbf{S}^{xx}$, $\mathbf{S}^{xy}$, $\mathbf{T}^{xxxx}$, etc., are the same for all elements and can be computed and stored. The $d\mathbf{K}_e^m/dA_{\rho\sigma}$ terms appearing in Eq. (C15) can be obtained similar to their bending counterparts.

Finally, the average strain displacement matrix as used in Eq. (5) for an square element with side s is computed from

$$\bar{\mathbf{B}}_e = \frac{1}{2s} \begin{bmatrix} -1 & 1 & 1 & -1 & 0 & 0 & 0 & 0 \\ 0 & 0 & 0 & 0 & -1 & -1 & 1 & 1 \\ -1 & -1 & 1 & 1 & -1 & 1 & 1 & -1 \end{bmatrix} \tag{B4}$$

Appendix C: Sensitivity Analysis

The sensitivity value in Eq. (13) is composed of two terms. The first term is local and can therefore be evaluated using information from a single element:

$$S_{b1} \equiv \mathbf{a}^T \cdot \frac{d\mathbf{K}^b}{db} \cdot \mathbf{a} = \mathbf{a}_i^T \cdot \frac{d\mathbf{K}_i^b}{db} \cdot \mathbf{a}_i \tag{C1}$$

The second term in Eq. (13) is not necessarily local. This is due to the fact that even when the stiffness of a single element is altered, the distribution of the in-plane loads is altered for all elements and thus the geometric matrices of all elements would change. In the following, an efficient way for the evaluation of this term is described.

Substituting from Eq. (3) into Eq. (13) and rearranging the terms S_{b2} is defined as

$$S_{b2} \equiv \mathbf{a}^T \cdot \frac{d\mathbf{K}^g}{db} \cdot \mathbf{a} = -\sum_e \mathbf{s}_e^T \cdot \frac{d\mathbf{n}_e}{db} \tag{C2}$$

where the vector $\mathbf{s}_e$ can be calculated locally as

$$\mathbf{s}_e = (\, \mathbf{a}_e^T \cdot \mathbf{K}_x \cdot \mathbf{a}_e, \quad \mathbf{a}_e^T \cdot \mathbf{K}_y \cdot \mathbf{a}_e, \quad \mathbf{a}_e^T \cdot \mathbf{K}_{xy} \cdot \mathbf{a}_e \,)^T \tag{C3}$$

The derivative of the in-plane stress resultants can be obtained by differentiation of Eq. (4) as

$$\frac{d\mathbf{n}_e}{db} = \frac{d\mathbf{A}_e}{db} \cdot \mathbf{e}_\mathbf{e} + \mathbf{A}_e \cdot \frac{d\mathbf{e}_\mathbf{e}}{db} \tag{C4}$$

Thus, the sum in Eq. (C2) can be decomposed into two terms corresponding to the two terms in Eq. (C4). The first term can be evaluated locally since only the in-plane stiffness matrix of the ith element depends on b. The second term involves the derivative of the average strain of an arbitrary element with respect to the change of stiffness of the ith element and is not local:

$$S_{b2} = -\mathbf{s}_i^T \cdot \frac{d\mathbf{A}_i}{db} \cdot \mathbf{e}_i - \sum_e \mathbf{s}_e^T \cdot \mathbf{A}_e \cdot \frac{d\mathbf{e}_e}{db} \tag{C5}$$

To evaluate the second term above, which is denoted by S_{b22} in Eq. (C5) term, Eq. (5) is differentiated with respect to b to obtain

$$\frac{d\mathbf{e}_\mathbf{e}}{db} = \bar{\mathbf{B}}_e \cdot \frac{d\mathbf{u}_e}{db} \tag{C6}$$

Thus the strain term S_{b22} simplifies to

$$S_{b22} = -\mathbf{g}_e^T \cdot \frac{d\mathbf{u}_e}{db} \tag{C7}$$

where the vector $\mathbf{g}$ is assembled from element contributions:

$$\mathbf{g}_e = \mathbf{B}_e^T \cdot \mathbf{A}_e \cdot \mathbf{s}_e \tag{C8}$$

The derivative of the in-plane displacement vector is obtained by differentiation of Eq. (6) as

$$\mathbf{K}^m \cdot \frac{d\mathbf{u}}{db} = -\frac{d\mathbf{K}^m}{db} \cdot \mathbf{u} \tag{C9}$$

Defining the adjoint displacement vector $\mathbf{v}$ as the solution of the problem

$$\mathbf{K}^m \cdot \mathbf{v} = -\mathbf{g} \tag{C10}$$

the strain term can be simplified to

$$S_{b22} = -\mathbf{v}^T \cdot \frac{d\mathbf{K}^m}{db} \cdot \mathbf{u}_\mathbf{e} \tag{C11}$$

which can be also evaluated locally.

Thus, all the calculations required to evaluate the sensitivity of the buckling load with respect to local change of stiffness of the ith element can be calculated using information at the element level. The global redistribution of loads is accounted for totally through the evaluation of the adjoint displacement vector $\mathbf{v}$. Substituting the above sensitivity equations back to Eq. (13), $\frac{d\lambda}{db}$ can be written as

$$\frac{d\lambda}{db} = \lambda\left(\mathbf{a}_i^T \cdot \frac{d\mathbf{K}_i^b}{db} \cdot \mathbf{a}_i\right) + \lambda^2\left(\mathbf{s}_i^T \cdot \frac{d\mathbf{A}_i}{db} \cdot \mathbf{e}_i + \mathbf{v}_i^T \cdot \frac{d\mathbf{K}_i^m}{db} \cdot \mathbf{u}_i\right) \tag{C12}$$

Keeping in mind that

$$\frac{\partial\lambda}{\partial\mathbf{S}^e} = -\mathbf{D}^e \cdot \frac{\partial\lambda}{\partial\mathbf{D}^e} \cdot \mathbf{D}^e \tag{C13}$$

and recalling that for the reciprocal approximation Eq. (17) the element sensitivities are decomposed into two separate bending and membrane parts as follows:

$$\Phi_{\alpha\beta}^{(b)^e} \equiv \frac{1}{\lambda^2}\frac{\partial\lambda}{\partial S_{\alpha\beta}^e} = \frac{1}{\lambda}\sum_{\sigma,\rho} D_{\beta\sigma} D_{\rho\alpha}\left(\mathbf{a}_e^T \cdot \frac{d\mathbf{K}_e^b}{dD_{\rho\sigma}} \cdot \mathbf{a}_e\right) \tag{C14}$$

and

$$\Psi_{\alpha\beta}^{(m)^e} \equiv \frac{1}{\lambda^2}\frac{\partial\lambda}{\partial A_{\alpha\beta}^e} = \sum_{\sigma,\rho}\left(\mathbf{s}_e^T \cdot \frac{d\mathbf{A}_e}{dA_{\rho\sigma}} \cdot \mathbf{e}_e + \mathbf{v}_e^T \cdot \frac{d\mathbf{K}_e^m}{dA_{\rho\sigma}} \cdot \mathbf{u}_e\right) \tag{C15}$$

where $\alpha, \beta, \sigma, \rho = 1 \ldots 3$ represent the components of the stiffness matrices of element e.

Similarly, when stiffness is maximized, the sensitivities of the compliance with respect to the in-plane stiffness is required. The compliance represents the energy stored within the structure such that

$$C = \frac{1}{2}\mathbf{u}^T \cdot \mathbf{K}^m \cdot \mathbf{u} = \frac{1}{2}\mathbf{f}^T \cdot \mathbf{u} \tag{C16}$$

Taking the derivative of Eq. (6) with respect to an arbitrary variable b and assuming that the applied force is a dead load, the derivative of the in-plane displacements is found to be

$$\frac{d\mathbf{u}}{db} = -(\mathbf{K}^m)^{-1} \cdot \frac{d\mathbf{K}^m}{db} \cdot \mathbf{u} \tag{C17}$$

Therefore the derivative of the compliance with respect to b can be expressed as

$$\frac{dC}{db} = -\frac{1}{2}\mathbf{u}^T \cdot \frac{d\mathbf{K}^m}{db} \cdot \mathbf{u} \tag{C18}$$

For the approximation of the compliance (19) the components of the sensitivity matrix thus become

$$\Phi_{\alpha\beta}^{(m)^e} = -\frac{\partial C}{\partial R_{\alpha\beta}} = -\frac{1}{2}\sum_{\sigma,\rho} A_{\beta\sigma} A_{\rho\alpha}\left(\mathbf{u}^T \cdot \frac{d\mathbf{K}^m}{dA_{\rho\sigma}} \cdot \mathbf{u}\right) \tag{C19}$$

Acknowledgment

This work is supported by the AUTOW (Automated Preform Fabrication by Dry Tow Placement) Project, part of the European Union Sixth Framework Program.

References

[1] Fukunaga, H., Sekine, H., Sato, M., and Iino, A., "Buckling Design of Symmetrically Laminated Plates Using Lamination Theory," *Computers and Structures*, Vol. 57, No. 4, 1995, pp. 643–649. doi:10.1016/0045-7949(95)00050-Q

[2] Grenestedt, J. L., "Layup Optimization Against Buckling of Shear Panels," *Structural optimization*, Vol. 3, No. 2, 1991, pp. 115–120. doi:10.1007/BF01743281

[3] Walker, M., Adali, S., and Verijenko, V., "Optimization of Symmetric Laminates for Maximum Buckling Load Including the Effects of Bending-Twisting Coupling," *Computers and Structures*, Vol. 58, No. 2, 1996, pp. 313–319. doi:10.1016/0045-7949(95)00138-7

[4] Hyer, M. W., and Lee, H. H., "The Use of Curvilinear-Fiber Format in to Improve Buckling Resistance of Composite Plates with Central Holes," *Composite Structures*, Vol. 18, No. 3, 1991, pp. 239–261. doi:10.1016/0263-8223(91)90035-W

[5] Gürdal, Z., and Olmedo, R., "In-Plane Response of Laminates with Spacially Varying Fiber Orientations: Variable Stiffness Concept," *AIAA Journal*, Vol. 31, No. 4, 1993, pp. 751–758. doi:10.2514/3.11613

[6] Tatting, B., and Gürdal, Z., "Design and Manufacture of Elastically Tailored Tow Placed Plates," NASA, TR CR-2002-211919, Aug. 2002.

[7] Lund, E., Kühlmeier, L., and Stegmann, J., "Buckling Optimization of Laminated Hybrid Composite Shell Structures Using Discrete Material Optimization," *6th World Congress on Structural and Multidisciplinary Optimization*, Rio de Janeiro, Brazil, 2005.

[8] Setoodeh, S., Abdalla, M. M., Gürdal, Z., and Tatting, B., "Design of Variable-Stiffness Composite Laminates for Maximum In-Plane Stiffness Using Lamination Parameters," *46th AIAA/ASME/ASCE/AHS/ASC Structures, Structural Dynamics & Materials Conference*, AIAA, Austin, TX, April 2005.

[9] Abdalla, M. M., Setoodeh, S., and Gürdal, Z., "Design of Variable Stiffness Composite Panels for Maximum Fundamental Frequency Using Lamination Parameters," *Composite Structures*, Vol. 81, No. 2, 2007, pp. 283–291. doi:10.1016/j.compstruct.2006.08.018

[10] Jegley, D. C., Tatting, B., and Gürdal, Z., "Tow-Steered Panels with Holes Subjected to Compression or Shear Loads," *46th AIAA/ASME/ASCE/AHS/ASC Structures, Structural Dynamics and Materials Conference*, Reston, VA, April 2005.

[11] Blom, A. W., Setoodeh, S., Hol, J. M. A. M., and Gürdal, Z., "Design of Variable-Stiffness Conical Shells for Maximum Fundamental Eigenfrequency," *Computers and Structures*, Vol. 86, No. 9, 2008,

pp. 870–878.
doi:10.1016/j.compstruc.2007.04.020
[12] Honda, S., Oonishi, Y., Narita, Y., and Sasaki, K., "Vibration Analysis of Composite Rectangular Plates Reinforced Along Curved Lines," *Journal of System Design and Dynamics*, Vol. 2, No. 1, 2008, pp. 76–86.10.1299/jsdd.2.76
[13] Alhajahmad, A., Abdalla, M. M., and Gürdal, Z., "Design Tailoring for Pressure Pillowing Using Tow-Placed Steered Fibers," *Journal of Aircraft*, Vol. 45, No. 2, 2008, pp. 630–640.
doi:10.2514/1.32676
[14] Setoodeh, S., Abdalla, M. M., IJsselmuiden, S. T., and Gürdal, Z., "Design of Variable-Stiffness Composite Panels for Maximum Buckling Load," *Composite Structures*, Vol. 87, No. 1, 2009, pp. 109-117.10.1016/j.compstruct.2008.01.008
[15] Tsai, S. W., and Pagano, N. J., "Invariant Properties of Composite Materials," *Composite Material Workshop*, Technomic, Westport, PA, 1968, pp. 233–252.
[16] Tsai, S. W., and Hahn, H. T., *Introduction of Composite Materials*, Technomic, Lancaster, PA, 1980.
[17] Lipton, R., "On Optimal Reinforcement of Plates and Choice of Design Parameters," *Control and Cybernetics*, Vol. 23, No. 3, 1994, pp. 481–492.
[18] Honda, S., and Narita, Y., "Design of Composite Panel with Optimally Distributed Short Fibers," *16th International Conference on Composite Materials*, Kyoto, Japan, 2007.
[19] Setoodeh, S., Blom, A. W., Abdalla, M. M., and Gürdal, Z., "Generating Curvilinear Fiber Paths from Lamination Parameters Distribution," *47th AIAA/ASME/ASCE/AHS/ASC Structures, Structural Dynamics, and Materials Conference*, Paper AIAA-2006-1875, Newport, RI, May 2006.
[20] Haftka, R., and Gürdal, Z., *Elements of Structural Optimization*, Kluwer Academic, Norwell, MA, 1992.
[21] Jones, R. M., *Mechanics of Composite Materials*, 2nd ed., Taylor and Francis, Washington, D.C., 1998.
[22] Hammer, V. B., Bendse, M. P., Lipton, R., and Pedersen, P., "Parametrization in Laminate Deign for Optimal Compliance," *International Journal of Solids and Structures*, Vol. 34, No. 4, 1997, pp. 415–434.
doi:10.1016/S0020-7683(96)00023-6
[23] Olmedo, R., and Gürdal, Z., "Buckling Response of Laminates with Spatially Varying Fiber Orientations," *AIAA/ASME/ASCE/AHS/ASC Structures, Structural Dynamics, and Materials Conference*, Reston, VA, 1993, pp. 2261–2269.
[24] Setoodeh, S., Abdalla, M. M., and Gürdal, Z., "Approximate Feasible Regions for Lamination Parameters," *11th AIAA/ISSMO Multidisciplinary Analysis and Optimization Conference*, Portsmouth, Virginia, 2006.
[25] Fleury, C., and Schmit, L. A. Jr., "Dual Methods and Approximation Concepts in Structural Synthesis," NASA, CR 3226, 1980.
[26] Setoodeh, S., Abdalla, M. M., and Gürdal, Z., "Design of Variable Stiffness Laminates Using Lamination Parameters," *Composites Part B*, Vol. 37, Nos. 4–5, 2006, pp. 301–309.
doi:10.1016/j.compositesb.2005.12.001
[27] Foldager, J., Hansen, J. S., and Olho, N., "A General Approach Forcing Convexity of Ply Angle Optimization in Composite Laminates," *Structural and Multidisciplinary Optimization*, Vol. 16, Nos. 2–3, 1998, pp. 201–211.
doi:10.1007/BF01202831
[28] Olhoff, N., "Multicriterion Structural Optimization via Bound Formulation and Mathematical Programming," *Structural optimization*, Vol. 1, No. 1, 1989, pp. 11–17.
doi:10.1007/BF01743805
[29] Seyranian, A. P., Lund, E., and Olhoff, N., "Multiple Eigenvalues in Structural Optimization Problems," *Structural optimization*, Vol. 8, No. 4, 1994, pp. 207–227.
doi:10.1007/BF01742705
[30] Rockafellar, R., "Monotone Operators and the Proximal Point Algorithm," *SIAM Journal Control and Optimization*, Vol. 14, No. 5, Aug. 1976, pp. 877–898.
doi:10.1137/0314056
[31] Gürdal, Z., Haftka, R., and Prabhat, H., *Design and Optimization of Laminated Composite Structures*, Wiley, New York, 1999.
[32] Van Campen, J., and Gürdal, Z., "Retrieving Variable Stiffness Laminates from Lamination Parameters Distribution," *50th AIAA/ASME/ASCE/AHS/ASC Structures, Structural Dynamics, and Materials Conference*, Paper AIAA-2009-2183, Palm Springs, CA, 4–7–May 2009.
[33] Reddy, J. N., *Mechanics of Laminated Composite Plates and Shells*, 2nd ed., CRC Press, Boca Raton, FL, 2004.

E. Livne
Associate Editor